Natural hyperfine and magnetic predissociation of the I2 B state III. - Experiments on magnetic predissociation

Jacques Vigué, M. Broyer, J.C. Lehmann

Classification
Physics Abstracts
33.60 — 33.80B — 33.80E — 82.50E

Natural hyperfine and magnetic predissociation of the I_2 B state III. — Experiments on magnetic predissociation

J. Vigué, M. Broyer and J. C. Lehmann

Laboratoire de Spectroscopie Hertzienne de l'E.N.S. (*), 24, rue Lhomond, 75231 Paris Cedex 05, France

(*Reçu le 19 novembre 1980, accepté le 25 mars 1981*)

Résumé. — Cet article présente l'ensemble des résultats expérimentaux actuellement disponibles sur la prédissociation magnétique de l'état B de l'iode. Ces résultats sont analysés grâce à la théorie de cette prédissociation. Les valeurs des paramètres de prédissociation magnétique, naturelle et hyperfine ainsi que la probabilité de décroissance radiative sont déduits des expériences. Les dépendances vibrationnelles et rotationnelles de ces paramètres sont mesurées et comparées à la théorie. La connaissance de la prédissociation de l'état B de I_2, telle qu'elle est présentée ici, semble maintenant presque complète.

Abstract. — This paper presents all experimental results presently available on the magnetic predissociation of the B state of I_2. These results are analysed according to the theory of this predissociation. The values of the parameters of the magnetic, natural, and hyperfine predissociation, and of the radiative decay rate are deduced from the experiments. The vibrational and rotational dependence of these parameters are measured and compared with theory. Experimental and theoretical knowledge of the I_2 B state predissociation, summarized here, now seems rather complete.

Introduction. — The magnetic quenching of the B $^3\Pi_{0^+u}$ state of I_2 was discovered experimentally by Steubing [1] in 1913 and by Wood and Ribaud in 1914 [2]. The theory of this phenomenon was given in terms of a magnetic predissociation by Turner [3] and Van Vleck [4]. Later on, various experiments were done [5, 6, 7] which confirmed this analysis. However in 1972-1974 we established [8, 9] the existence of an interference effect between the natural and magnetic predissociations of the I_2 B state and we gave a new analysis of this predissociation [10]. Since that work many new facts have appeared and require a more complete analysis :

— the discovery of a hyperfine predissociation [11] which also interferes with the magnetic predissociation ;

— we have studied [12] the magnetic predissociation of a large number of rovibrational levels ;

— as is explained in the second paper [13] of this series, the J dependence of the Franck-Condon density for predissociation is not negligible and should be taken into account in the calculations.

Before going into any detail, we summarize the interesting aspects of a study of magnetic predissociation :

i) it is one of the rare cases in which a coupling between a discrete level and a continuum can be tuned ;

ii) the interference between magnetic and gyroscopic predissociation enables us to measure very weak gyroscopic predissociation rates ;

iii) the experiments are quite simple : a variation of the magnetic field produces a variation of the fluorescence quantum yield and therefore of the fluorescence light intensity.

The present publication is divided into four parts : the first is devoted to an historical review of previous results and a brief survey of the present theory. The second part describes the experimental consequences of the predissociation rate calculations. The third one gives a detailed account of all experiments and their numerical analysis. The last part summarizes the results obtained and presents a tentative interpretation of the parameters.

1. **Historical review. Present theory.** — 1.1 First observations and Van Vleck theory. — In 1913 Steubing [1], followed in 1914 by Wood and Ribaud [2], observed magnetic quenching of the fluorescence

(*) Associé au C.N.R.S.

of I_2. The quenching was very strong for a magnetic field of 30 kG and a low iodine pressure (about 30 mtorr); and it was negligible for the same field and a pressure of the order of 1 torr.

Various studies were made, which gave a quantitative form to these results. Moreover, Turner [3] determined the dependence of the effect on the excitation wavelength, and proposed, in view of the rapid dependence observed, that the effect was a field induced predissociation. Van Vleck [4] gave a detailed theory of such a predissociation and identified the symmetry of the dissociative state as 0_u^-; this choice was dictated by the consideration that the other possible symmetry, 1_u could also participate in a natural gyroscopic predissociation ($\Gamma_{pred} \propto J(J+1)$), which would obscure the magnetic predissociation, at least for large rotational quantum number J. The magnetic predissociation rate was given as [4, 5]

$$\Gamma_{pred} = b_v B^2 \qquad (1)$$

and the fluorescence yield is therefore proportional to

$$\rho_f = \frac{\Gamma_{rad}}{\Gamma_{rad} + \Gamma_{coll} + b_v B^2} \qquad (2)$$

where Γ_{rad} and Γ_{coll} are the radiative and collisional decay rates. The behaviour predicted by equation (2) was verified by various authors, a list of whom is given in reference [5]. This reference contains one of the most detailed studies : the validity of equations (1) and (2) was carefully tested and the vibrational dependence of b_v was measured in the region $v > 13$. This work was extended by Chapman and Bunker [6] who determined the predissociation of the two levels ($v=6$, $J = 32$ and $v = 11$, $J = 128$) excited by the HeNe laser; they showed that the b_v *vs.* v curve has two maxima, one around $v = 6$ and one around $v = 25$ and that b_v vanishes for $v = 14$. Figure 1 shows the b_v curve thus obtained. Finally, a direct lifetime measurement as a function of the magnetic field was made by Capelle and Broida [7]. They verified that the lifetime τ is correctly given by

$$\frac{1}{\tau} = \Gamma_{rad} + \Gamma_{coll} + b_v B^2 ,$$

their b_v values being in good agreement with the other determinations.

1.2 First observations of the interference between magnetic and gyroscopic predissociations. — While studying the magnetic quenching effect, we observed that a circular polarization of the fluorescence light was obtained, following a linearly polarized excitation, in the presence of a magnetic field [8]. It was easily verified that this was due to different fluorescence quantum yield for the Zeeman sublevels of $+M$ and $-M$ values. We presented [8, 9, 10] a theory explaining this difference as due to an interference effect between the magnetic and

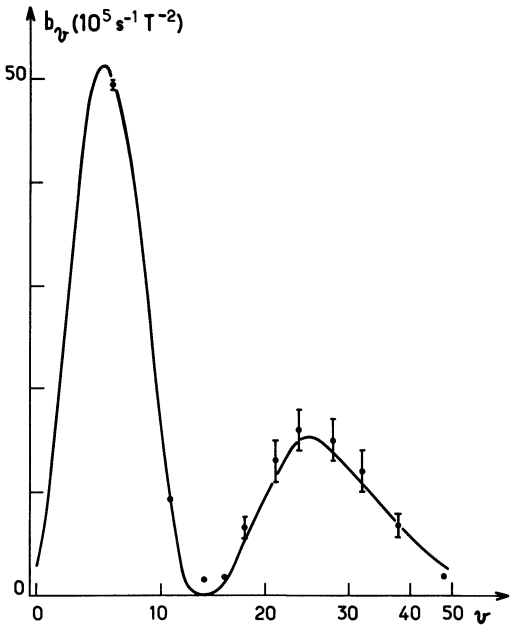

Fig. 1. — This figure presents the results of Chapman and Bunker [6]. The points are the experimental b_v values, and the full curve is the best theoretical curve obtained by fitting the 1_u state potential curve. The horizontal scale is linear in vibrational energy.

natural predissociation of the B state. Such an interference term exists only if the natural and magnetic predissociations are both due to the same state, whose symmetry is then necessarily 1_u. The details of the theory, and various considerations (namely the elimination of spurious effects which could contribute to the observed polarization) appeared in previous publications [8, 9, 10].

We now know that our original theory [10] is only a particular case of the general theory which includes hyperfine predissociation. Evidently, this first theory is unsatisfactory. Its main drawback is due to the absence of the hyperfine predissociation effect. Therefore the hyperfine predissociation is actually more or less included in the radiative decay rate, and this apparent radiative decay rate varies rapidly with J for one vibrational level [12].

1.3 The present theory. — A detailed theory appears in the first paper of this series [14]. Let us recall briefly that the predissociation rate of the level $| vJ\varepsilon FM_F \rangle$ is given by :

$$\Gamma_p(v, J, \varepsilon, F, M_F) = \Gamma_{nat} + \Gamma_{mag} + \Gamma_{int} . \qquad (3a)$$

In this expression, Γ_{nat} is the natural predissociation rate. This term has been studied in detail in the second paper of this series. It can be written, with some simplifying assumptions

$$\Gamma_{nat} = \sum_I | \alpha(I\varepsilon JF) |^2 \Gamma_{IJF} , \qquad (3b)$$

with

$$\Gamma_{IJF} = C_v^2 J(J+1) + \frac{a_v^2}{3}\left(\mathbf{I}^2 + \frac{3(\mathbf{I}.\mathbf{J})^2 + \frac{3}{2}(\mathbf{I}.\mathbf{J}) - \mathbf{I}^2\,\mathbf{J}^2}{(2J-1)(2J+3)}\right) - a_v\, C_v \sqrt{2}\,\mathbf{I}.\mathbf{J}\,. \quad (3c)$$

Γ_{mag} is the purely magnetic term; it is given by :

$$\Gamma_{\text{mag}} = \sum_I |\, \alpha(I\varepsilon JF)\,|^2\, \Gamma_{ZZ}(vJIFM_F) \quad (3d)$$

with

$$\Gamma_{ZZ}(v, J, I, F, M_F) = (\alpha_v B)^2 \times \frac{1}{3} \times \left[1 + \frac{2(3M_F^2 - F(F+1))}{F(F+1)} \times \frac{3(\mathbf{J}.\mathbf{F})^2 - \frac{3}{2}\mathbf{J}.\mathbf{F} - \mathbf{F}^2\,\mathbf{J}^2}{(2F-1)(2F+3)(2J-1)(2J+3)}\right]. \quad (3e)$$

This term is quadratic in B and an even function of M_F.

Γ_{int} is the interference term between the magnetic and natural predissociations. This term is linear in B and an odd function of M_F

$$\Gamma_{\text{int}} = \sum_I |\, \alpha(I\varepsilon JF)\,|^2\, (\Gamma_{ZG} + \Gamma_{GZ} + \Gamma_{ZHFS} + \Gamma_{HFSZ})_{(vJIFM_F)} \quad (3f)$$

$$(\Gamma_{ZG} + \Gamma_{GZ})_{(vJIFM_F)} = \sqrt{2}\,\alpha_v\, BC_v\, M_F \frac{\mathbf{FJ}}{\mathbf{F}^2} \quad (3g)$$

$$(\Gamma_{ZHFS} + \Gamma_{HFSZ})_{(vJIFM_F)} = -\,\alpha_v\, Ba_v \frac{M_F}{F(F+1)} \times \frac{2}{3}\left[\mathbf{I}.\mathbf{F} + \frac{3(\mathbf{F}.\mathbf{J})(\mathbf{J}.\mathbf{I}) - \mathbf{J}^2(\mathbf{I}.\mathbf{F})}{(2J-1)(2J+3)}\right]. \quad (3h)$$

In all cases, C_v, a_v, α_v are proportional to the Franck-Condon density for predissociation, and therefore are J dependent, as has been shown in the previous paper [13]. In equation (3) we must replace C_v, a_v, α_v by C_{vJ}, a_{vJ}, α_{vJ} everywhere, or we must introduce the multiplicative factor $[1 + p_v\, J(J+1) + q_v[J(J+1)]^2]$; C_v, a_v, α_v then designating the value of the coefficient for $J = 0$.

Therefore Γ_p appears to be a function of $v, J, \varepsilon, F, M_F$. This relaxation rate is different for each M_F sublevel, and in particular, it is not the same for two levels having the same values of $vJ\varepsilon F$ and opposite signs of M_F. This last point is the crucial difference between Van Vleck's [4] and the present theory.

2. **Experimental consequences of the theory.** — We consider here the experiments in which we detect the polarization or the intensity of the fluorescence light as a function of magnetic field. It will appear that the qualitative predictions of the theory ignoring hyperfine predissociation [10] are preserved, but the quantitative relations established then are not valid.

2.1 FLUORESCENCE INTENSITY AS A FUNCTION OF MAGNETIC FIELD. — Using the well known master equation formalism, one can write, for the density matrix of the excited states :

$$\frac{d\rho}{dt} = \frac{1}{i\hbar}[\mathcal{H}, \rho] - \frac{1}{2}(\Gamma\rho + \rho\Gamma) + \frac{\mathcal{E}}{T_p}, \quad (4)$$

$\mathcal{H}$ is the sum of the hyperfine and the Zeeman hamiltonians, $\mathcal{E}$ is the excitation operator [15], which depends on the exciting light beam polarization and the nature of the excitation transition (P or R). T_p is the pumping time and Γ is the relaxation matrix :

$$\Gamma = \Gamma_{\text{rad}} + \Gamma_{\text{coll}} + \Gamma_{\text{pred}}\,; \quad (5)$$

Γ_{rad}, corresponding to decay by spontaneous emission of radiation, is perfectly isotropic; Γ_{coll}, corresponding to relaxation by collision is not very well known. In the I_2 B state all our experiments [12] seem to prove that for I_2-I_2 collisions, it is a good approximation to consider this process as isotropic. Γ_{rad} and Γ_{coll} are then two scalar matrices. Γ_{pred} is diagonal in the $J\varepsilon FM_F$ basis and its matrix elements are simply :

$$\langle J\varepsilon FM_F \,|\, \Gamma_{\text{pred}} \,|\, J\varepsilon' F' M_F' \rangle = \delta_{\varepsilon\varepsilon'}\,\delta_{FF'}\,\delta_{M_F M_F'}\,\Gamma_p(v, J, \varepsilon, F, M_F)\,. \quad (6)$$

The fluorescence intensity is simply given by

$$\mathfrak{I} \propto \text{Tr}\,(\rho\mathfrak{D})\,, \quad (7)$$

where $\mathfrak{D}$ is the detection operator [15]. $\mathfrak{D}$ is very similar to $\mathcal{E}$ and depends on the polarization of the detection light beam, and also on the nature (P or R) of the transition used in the detection. To calculate $\mathcal{E}$ and $\mathfrak{D}$ we use their decomposition into irreducible tensorial sets [16].

Up to now, these equations are perfectly general, and could be applied to time resolved as well as to stationary state experiments. We consider, from now on, only experiments under stationary state conditions and, moreover, we choose the geometry so that

no Hanle effect or level crossing signal can be observed. This means that either $\mathfrak{D}$ or $\mathfrak{E}$ is diagonal in the eigenstate basis ; we suppose that the zero field basis set $| J\varepsilon FM_F \rangle$ represents well the eigenstates of $\mathcal{H}$ in the region of magnetic field explored (i.e. we neglect all hyperfine decoupling). Then we get

$$\mathfrak{I} \propto \sum_{\varepsilon FM_F} \frac{\langle J\varepsilon FM_F | \mathfrak{D} | J\varepsilon FM_F \rangle \langle J\varepsilon FM_F | \mathfrak{E} | J\varepsilon FM_F \rangle}{\Gamma_{\text{rad}} + \Gamma_{\text{coll}} + \Gamma_{\text{p}}(vJ\varepsilon FM_F)} \tag{8}$$

with

$$| J\varepsilon FM_F \rangle = \sum_I \alpha(I\varepsilon JF) | JIFM_F \rangle . \tag{9}$$

Although this expression seems easy to evaluate, for a typical J value ($J = 100$ for instance) the summation over εFM_F involves about 4 000 terms ! We must therefore try to minimize the amount of computation : this is done by remarking that $\mathfrak{I}$ depends only on some combinations of all the parameters involved in equation (8). As we consider only relative intensities, we may define $\mathfrak{I}$ by the following equation

$$\mathfrak{I} = \sum_{\varepsilon FM_F} \frac{\langle J\varepsilon FM_F | \mathfrak{D} | J\varepsilon FM_F \rangle \langle J\varepsilon FM_F | \mathfrak{E} | J\varepsilon FM_F \rangle}{1 + \dfrac{\Gamma_{\text{p}}(v, J, \varepsilon, F, M_F)}{\Gamma_{\text{rad}} + \Gamma_{\text{coll}}}} . \tag{10}$$

In equation (10), it is clear that $\mathfrak{I}$ depends

— on the geometry of the experiment and on the nature of the excitation and detection transitions through $\mathfrak{E}$ and $\mathfrak{D}$;

— on the following combinations of parameters :

$$\frac{C_{vJ}}{\sqrt{\Gamma}}, \quad \frac{a_{vJ}}{\sqrt{\Gamma}}, \quad \frac{\alpha_{vJ} B}{\sqrt{\Gamma}},$$

where Γ designates the sum $\Gamma_{\text{rad}} + \Gamma_{\text{coll}}$;

— on the value of J and on its parity which gives the ortho or para nature of the level ;

— on the hyperfine structure of the level which determines the α coefficients.

If J is large when compared to the nuclear spin (5/2 for ^{127}I), one finds [4, 12] that $C_{vJ}/\sqrt{\Gamma}$ and J appear only through their product $C_{vJ} J/\sqrt{\Gamma}$.

Finally, in the case where the excitation is not done with a line broader than the hyperfine structure, we must introduce into equation (10) a weight factor $w_{\varepsilon F}$ which takes into account the variation of excitation efficiency from one hyperfine level to another. We have chosen to neglect the magnetic tuning effects : indeed this should be negligible if the laser line is well centred on the absorption line, because the Landé factor of iodine in the B state is very small for the low vibrational levels (in these experiments, v is always smaller than 40, and in a large majority of cases $v \leqslant 22$).

2.2 Results of the calculations. — We have written a computer code which evaluated $\mathfrak{I}$ in the general case ; this computer routine was used to generate theoretical curves which are discussed here, and to fit the experimental data (see part 3). We are going to consider only two different experiments :

a) Excitation with linearly polarized light (σ or π : i.e. perpendicular or parallel to the magnetic field) and detection of circularly polarized light intensity $I_{\sigma^+} - I_{\sigma^-}$.

b) Excitation with σ linearly polarized light and detection of the total fluorescence intensity $I_{\sigma^+} + I_{\sigma^-}$.

The figures 2*a* and 2*b* give some plots of typical curves obtained for these two experiments. We analyse, in the following pages, the main characteristics of these two signals.

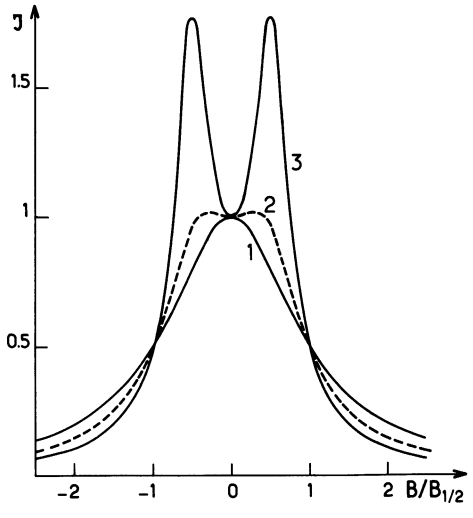

Fig. 2*a*. — This figure presents the calculated total fluorescence intensity $\mathfrak{I} = I_{\sigma^+} + I_{\sigma^-}$ as a function of the magnetic field B in the case of σ linearly polarized excitation. The curves are normalized to 1 in zero field and a reduced magnetic field scale is used ; $B_{1/2}$ is the field for which the intensity is the half of the intensity in zero field. For all curves $a_{vJ} = 0$ and $C_{vJ} J/\sqrt{\Gamma}$ is equal to : 0 (curve 1) ; 1 (curve 2) ; 3 (curve 3).

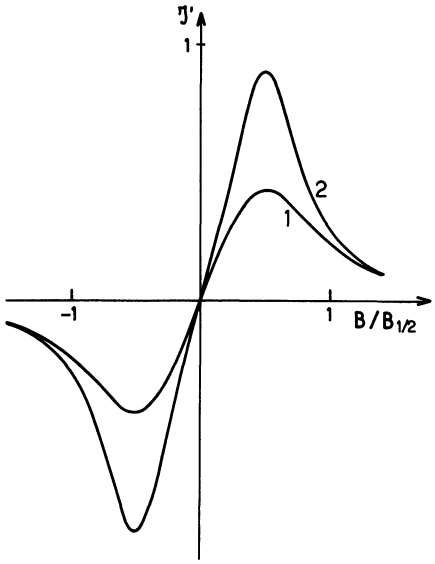

Fig. 2b. — The calculated circularly polarized intensity

$$J' = (I_{\sigma^+} - I_\sigma)_B/(I_{\sigma^+} + I_\sigma)_{B=0}$$

as a function of the magnetic field B (same scale as in 2 a; σ linearly polarized excitation). $a_{vJ} = 0$ and $C_{vJ} J/\sqrt{\Gamma}$ is equal to 1 (curve 1); 2 (curve 2).

Experiment a

We define a circular polarization « rate » θ by the following equation

$$\theta = \frac{(I_{\sigma^+} - I_\sigma)_{\max}}{(I_{\sigma^+} + I_\sigma)_{B=0}}. \qquad (11)$$

The choice of this quantity is a matter of experimental convenience and θ, thus defined, may exceed 1. Evidently, θ is a function of the following :

— nature (R or P) of the excitation and detection transitions;

— polarization σ or π of the exciting light beam;

— the combination of parameters (J is assumed to be large) :

$$\frac{a_{vJ}}{\sqrt{\Gamma}}, \quad \frac{C_{vJ} J}{\sqrt{\Gamma}};$$

— the parity of J.

We are going to discuss briefly these various dependences.

i) *Nature of the transitions used for excitation and detection.* — The measurement of $(I_{\sigma^+} - I_\sigma)$ gives a measurement of the longitudinal orientation ρ_0^1. When changing from an R line to a P line in detection, the detection factor for this orientation changes sign, but keeps almost the same modulus, if the rotational quantum number J is large enough. This can be understood on a classical basis [18]. Changing the nature of the excitation line affects the excitation matrix slightly and also the value of θ.

We have compared the modulus of θ in the various cases : the largest one is for the R ↑ R ↓ configuration and the smallest for the P ↑ P ↓ one. For large J values ($J \geqslant 20$) and a zero value of a_v, we get :

$$\left|\frac{\theta_{RR}}{\theta_{PP}}\right| \approx 1 + \frac{1.25}{J}. \qquad (12)$$

This is a small effect, and as θ was usually measured only for levels with $J > 30$, this explains our failure to observe any difference between the various RP configurations (except the change of sign when going from R to P detection).

ii) *Effect of the polarization π or σ of the exciting light beam.* — The circular polarization of the fluorescence is due to the lifetime difference between the $+ M_F$ and $- M_F$ sublevels; as this difference is due to the interference terms (eqs. (3f, g, h)) linear in M_F, this effect is certainly sensitive to changes in the relative populations of M_F sublevels. It is easy to verify that, for an R or P transition, a σ linear polarization produces a maximum population for $M_F = \pm F$ and a minimum population for $M_F = 0$: whereas a π polarization does the opposite. We expect therefore θ_π to be smaller than θ_σ. We have calculated θ_π and θ_σ for various values of $C_v J/\sqrt{\Gamma}$ and $a_v/\sqrt{\Gamma}$. The ratio θ_π/θ_σ is not constant, but if we limit the investigation to the values of these parameters accessible in the I_2 B state, we find :

$$0.48 \leqslant \frac{\theta_\pi}{\theta_\sigma} \leqslant 0.62. \qquad (13)$$

As only very few experiments concern θ_π, we do not give any more details. Clearly θ_σ which is larger, and therefore easier to measure, is more interesting to study.

iii) *Dependence on the parameters J, $C_{vJ}/\sqrt{\Gamma}$, $a_{vJ}/\sqrt{\Gamma}$.* — If J is large, we may reduce this set of three parameters to two alternative sets of two parameters :

— $C_{vJ} J/\sqrt{\Gamma}$, $a_{vJ}/\sqrt{\Gamma}$;

— $C_{vJ} J/\sqrt{\Gamma}$, $y_J = a_{vJ}/(C_{vJ} J) = Y/J$.

In both cases we must not forget the ortho para nature of the level. Figure 3 represents the curves

$$\theta_\sigma = f(C_{vJ} J/\sqrt{\Gamma})$$

with either $a_{vJ}/\sqrt{\Gamma}$ constant (3a) or y_J constant (3b).

In the first case θ is an almost linear function of $C_{vJ} J/\sqrt{\Gamma}$, the slope being dependent on $a_v/\sqrt{\Gamma}$. This means that for a vibrational level in which a_{vJ} and C_{vJ} are almost independent of J, θ should be a linear function of J.

In the second case, θ increases at first with $C_{vJ} J/\sqrt{\Gamma}$ and then saturates. It is very important to note that the saturation value of θ is strongly dependent on y_J.

In both cases, θ appears to be very different for ortho and para states, especially for broad line excitation (not shown in Fig. 3); however, this difference is completely washed out in the case of single

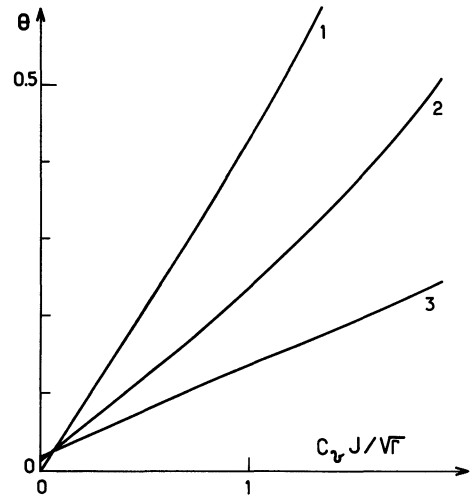

Fig. 3*a*. — The calculated rate of polarization θ_σ as a function of $C_{vJ} J/\sqrt{\Gamma}$ for various values of $a_{vJ}/\sqrt{\Gamma}$: 0 (curve 1); — 0.4 (curve 2); — 0.8 (curve 3). The rotational state is assumed to be ortho.

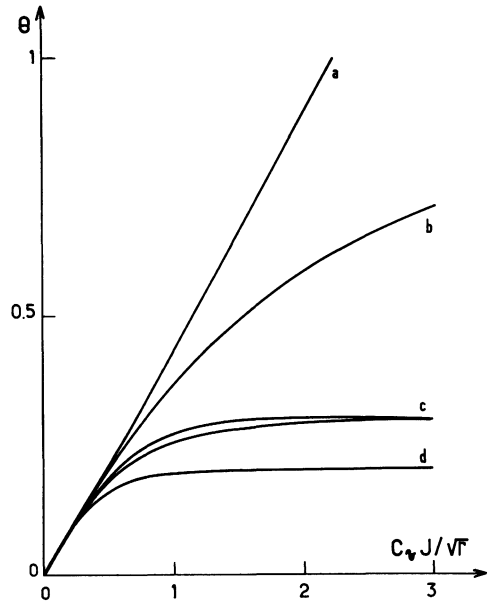

Fig. 3*b*. — The calculated rate of polarization θ_σ as a function of $C_{vJ} J/\sqrt{\Gamma}$ for various value of $y_J = a_{vJ}/(C_{vJ} J) = 0$ (curve a); — 0.175 (curve b); — 0.350 (curve c); — 0.50 (curve d). All the curves are calculated for ortho states, except curve c which contains two branches : the upper one for para states, the lower one for ortho states.

mode laser excitation. This is to be expected : the hyperfine sublevels which are responsible for the largest difference between ortho and para states are mainly in the wings of the line and their weight factors are very small.

From this study, it is clear that θ provides a measure of $C_v J/\sqrt{\Gamma}$ if this quantity is not too large and if $a_v/\sqrt{\Gamma}$ is known. When $C_v J/\sqrt{\Gamma}$ is large, the value of θ determines $y_J = Y/J$ and this is a new means of access to the parameter $Y = a_v/C_v$.

Experiment b

In this experiment, we observe the total fluorescence intensity $I_{\sigma^+} + I_{\sigma^-}$ as a function of the magnetic field, the excitation beam being σ linearly polarized.

The importance of such an experiment appears with the three following considerations :

— It is easy to perform the experiment : the signal is essentially the same whatever the combination of R or P lines used for excitation and detection, and therefore it is not necessary to discriminate R *vs.* P fluorescence lines. This gives a high fluorescence intensity and the signal to noise ratio is usually good, and in all cases better than in experiment a.

— This experiment allows a sensitive measurement of the predissociation parameter α_v, if the parameters Γ, a_v, C_v are already known.

— Finally, this experiment was the only one performed in the past [1, 2, 3, 5, 6] and in all cases the fluorescence intensity was found to be a Lorentz function of the magnetic field. As is shown in figure 2, this is no longer true in the present theory and it seems important to investigate this point in greater detail.

The curve $\mathcal{I} = I_{\sigma^+} + I_{\sigma^-} = f(B)$ is a particular case of equation (10); in this case only the population ρ_0^0 and the longitudinal alignment ρ_0^2 contribute to the signal. The excitation and detection factors for these quantities have a constant sign when going from an R to a P line, and their modulus is only slightly affected by this change if J is large. Therefore, the curve, its shape, and its width are only slightly affected by the nature of the lines used for excitation and detection.

i) *Width of the curve.* — From the study of equation (10), it appears that the half width $B_{1/2}$ (defined as the value $B_{1/2}$ such that $f(B_{1/2}) = f(B = 0)/2$) can be written as

$$\frac{\alpha_{vJ} B_{1/2}}{\sqrt{\Gamma}} = g\left(J, \frac{C_{vJ}}{\sqrt{\Gamma}}, \frac{a_{vJ}}{\sqrt{\Gamma}}\right). \tag{14}$$

The function g can be computed only numerically, except in the case $a_{vJ} = C_{vJ} = 0$, in which an approximate summation [19] restores the validity of equation (2) :

$$\mathcal{I} = \frac{\mathcal{I}_0}{1 + \dfrac{(\alpha_{vJ} B)^2}{3\,\Gamma}} \tag{15}$$

giving

$$b_v = \alpha_{vJ}^2/3 \tag{16}$$

and

$$B_{1/2}^{*} = \sqrt{3\,\Gamma}/\alpha_{vJ}\,. \tag{17}$$

In the general case, we may use numerical values of $B_{1/2}$ or more conveniently of $\alpha_{vJ} B_{1/2}/\sqrt{\Gamma}$. The variation of this last quantity is plotted as a function of $C_{vJ}^2 J^2/\Gamma$ for a typical set of values of $a_v/\sqrt{\Gamma}$ in

figure 4. We see on this figure that $B_{1/2}$ increases rapidly with $C_{vJ}^2 J^2/\Gamma$ (this a proof of the sensitivity of $B_{1/2}$ to C_{vJ}) and $B_{1/2}$ is not the same for ortho and para states (which is the proof of the sensitivity of $B_{1/2}$ to a_{vJ}). These behaviours have indeed been verified experimentally, but it is difficult to use them to derive new values of C_{vJ} and a_{vJ}.

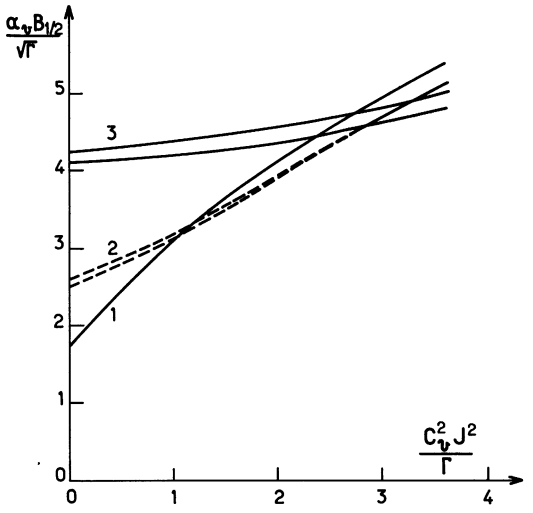

Fig. 4. — Plot of the calculated values of $\alpha_{vJ} B_{1/2}/\sqrt{\Gamma}$ as a function of $C_{vJ}^2 J^2/\Gamma$ for various values of $a_{vJ}/\sqrt{\Gamma}$: 0 (curve 1), -0.4 (curve 2), -0.8 (curve 3). In each case the lower curve is for para states, the upper for ortho states; when $a_v = 0$, there is no difference between the two curves.

ii) *Shape of the curve.* — Figure 2*a* has shown some typical curves $\mathfrak{I} = f(B)$. If $C_{vJ} J/\sqrt{\Gamma}$ and $a_{vJ}/\sqrt{\Gamma}$ are both much smaller than 1, the curve is almost a perfect Lorentzian. In the opposite case, for a certain range of values of $C_{vJ} J/\sqrt{\Gamma}$ and $a_v/\sqrt{\Gamma}$, the curve exhibits a maximum at nonzero magnetic field (see Fig. 2). In this case we may define a measure of the deviation by $\mathcal{R} = \mathfrak{I}_m/\mathfrak{I}(0)$, where $\mathfrak{I}_m$ is the value of this maximum and $\mathfrak{I}(0)$ the value of $\mathfrak{I}$ in zero field.

The origin of this effect is the following : if the natural gyroscopic predissociation is large enough, in zero magnetic field the fluorescence quantum yield is small. Then, when the field increases, the quantum yield decreases for some levels and increases for the others, depending on the sign of $M_F B$. Obviously the largest quantum yield decrease cannot exceed the initial yield, whereas the largest possible gain is to restore a unity quantum yield. Therefore, the gains may be larger than the losses and the average effect may be an increase in the fluorescence yield.

In figure 5 we have plotted the curves of equal $\mathcal{R}$ values as a function of $C_v J/\sqrt{\Gamma}$ and $a_v/\sqrt{\Gamma}$ for ortho and para states. For a fixed value of $C_v J/\sqrt{\Gamma}$, $\mathcal{R}$ is always a decreasing function of $|a_v|/\sqrt{\Gamma}$. Similarly, $\mathcal{R}$ is smaller for an ortho state than for a para state.

3. **The experiments and their analysis.** — In order to test the validity of the present theory and to measure

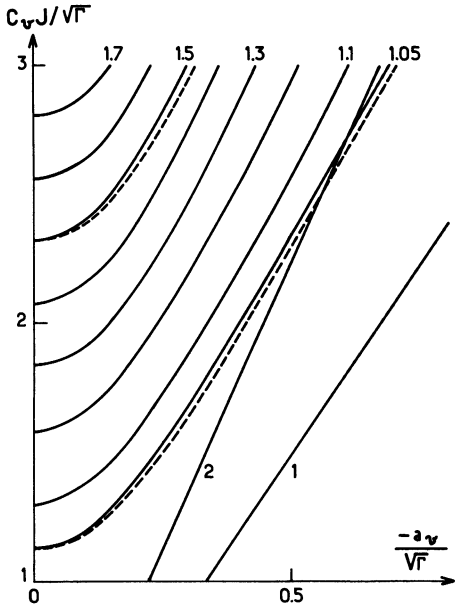

Fig. 5. — Curves for equal $\mathcal{R}$ value in the plane $C_{vJ} J/\sqrt{\Gamma}$, $a_{vJ}/\sqrt{\Gamma}$. The full lines correspond to ortho states and the dotted lines, given only for $\mathcal{R} = 1.05$ and 1.5, to para states. The straight lines numbered 1 and 2 represent respectively the case of levels having $J = 100$ (1) and 150 (2), the ratio $a_v^2/C_v^2 = Y^2$ being taken equal to 1 120 ($Y < 0$). Clearly, reaching $\mathcal{R} > 1.05$ necessitates a very high J value and a large predissociation, and is easier in a para than in an ortho level.

predissociation parameters, a large number of experiments have been performed. Most of these experiments are systematic studies of selectively excited rovibrational levels. We describe first the set up, then the experiments, and finally we analyse the results.

3.1 EXPERIMENTAL SET UP. — A laser is used to excite a low pressure iodine vapour contained in a sealed cell placed between the poles of an electromagnet which can provide a field up to 1.8 tesla. A side arm of the cell is cooled and its temperature controls the iodine pressure in the range 3-200 mtorr. The laser beam, linearly polarized and expanded to avoid saturation effects, passes through the cell. The fluorescence light, emitted at right angles in the direction of the magnetic field is circularly analysed and reflected into a grating monochromator (focal length 750 mm, resolving power 20 000) and then is detected by a magnetically shielded photomultiplier. We have verified that the residual variation of photomultiplier sensitivity due to the stray magnetic field is less than 1 %.

The laser beam is modulated at 80 Hz by a mechanical chopper; the resultant modulation of the P.M. current is detected by a phase sensitive detector. The intensity of the laser is measured and the fluorescence signal is divided by the laser intensity in order to eliminate the effects of laser power drifts.

The magnetic field is measured by a rotating coil magnetometer calibrated *versus* a nuclear magnetic resonance.

With this apparatus, we can plot three different types of signals :

— fluorescence spectra by sweeping the monochromator;

— fluorescence intensity for one circular polarization I_{σ^+} (or I_{σ^-}) as a function of the magnetic field;

— total fluorescence intensity $I_{\sigma^+} + I_{\sigma^-}$ as a function of the magnetic field (by removing the circular analyser).

3.2 THE LASER SOURCES. — In some earlier experiments, we used fixed frequency multimode lasers (Ar^+, Kr^+ and HeNe). However, most experiments were done with tunable, single mode dye lasers.

The choice of this second type of laser was dictated by the high density of the iodine spectrum [20] (about 10 intense lines per Å). The use of a single mode laser permits the excitation of any line, even a very weak one, without any problem due to an intense neighbouring line. We use Spectra Physics dye lasers model 580 and 580 A pumped by a 4 W all lines Ar^+ laser. With the Rhodamines 110, 6 G and B, we covered the range 5 380-6 425 Å almost continuously.

The drawbacks to the use of a single mode laser are the following :

— the excitation probability is not the same for all hyperfine sublevels, as the Doppler half width is about 250 MHz, and the total hyperfine structure of a line covers 900 MHz;

— some magnetic tuning effects could distort the magnetic predissociation effects; however, if the laser line is well centred on the absorption line, there is a very good cancellation of magnetic tuning effects, as was verified on a predissociation-free level.

The wavenumber of the laser is measured with the monochromator used for fluorescence detection and with a 1 mm thick air spaced Fabry-Pérot. With frequent calibration of this apparatus, using spectral lamps and lasers, the wavenumber of the tunable laser is easily determined with an uncertainity of about $\pm$ 0.15 cm^{-1}.

3.3 SERIES OF MEASUREMENTS. — About 185 rovibrational levels have been examined. The vibrational quantum number v varied in the range 4-39 and the rotational quantum numbers were usually in the range 25-140; however $J = 174$ was reached on one occasion. The limitation on the range of v is mainly due to the limitation of the spectral range of our lasers and also to the very small values [22] of Franck-Condon factors connecting the well populated v'' levels to the lowest v' levels.

The large majority of the levels studied (160 out of 185) lie in the range $v' = 4 - 22$. We will use also some lifetime measurements done with Ar^+ and Kr^+ lasers on the levels $v' = 40, 43, 62, 70$. No magnetic predissociation study was made with v' larger than 40. Clearly, due to the increasing values of the Landé factors [17], magnetic tuning effects should make such studies very difficult.

In all cases, a fluorescence spectrum was recorded; the rotational structure was resolved; its value gave an approximate measurement of the rotational quantum number. It was also possible to determine the R or P nature of the absorption line. The Franck-Condon pattern observed in the fluorescence intensities identified the vibrational quantum number v'. The calculation of the absorption line wavenumbers using the iodine constants [23] available at the time of these experiments (1976-1977) and the accurate wavenumber of the laser gave a few possible identifications for the absorption transition : among them only one was, in all cases, in agreement with the information deduced from the fluorescence spectrum. Then the identification of the excited state was complete.

We always recorded a curve $I_{\sigma^+} + I_{\sigma^-} = f(B)$ on an unresolved fluorescence doublet, chosen among the most intense members of the vibrational progression. Then, in most cases, a curve $I_{\sigma^-} = f(B)$ was recorded successively on the R line, then on the P line of this doublet. These curves we recorded for an iodine pressure $p = 30$ mtorr, corresponding to a cold point temperature of 0 °C, which had the advantage of being easy to maintain and gave a sufficient fluorescence signal. Simultaneously, the collisional decay rate Γ_{coll} is not too large and easy to calculate, as the cross-sections are well known [24, 25].

In some cases, the same curves were recorded for various pressures in the range 3-200 mtorr.

In all cases we have verified that the laser intensity was not so high as to produce saturation effects, which would invalidate formulae (4)-(10).

To give an idea of the quality of the signal observed, we show in figure 6 a curve $I_{\sigma^+} + I_{\sigma^-} = f(B)$ and a curve $I_\sigma = f(B)$. The signal to noise ratio is rather good and should not limit the accuracy of the interpretation.

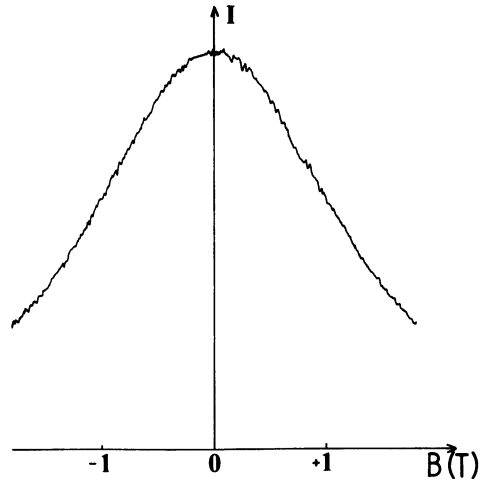

Fig. 6a. — Example of an experimental curve $I_{\sigma^+} + I_{\sigma^-} = f(B)$ recorded for the level $v' = 10$ $J' = 56$ with an iodine pressure of 30 mtorr. The magnetic field is measured in teslas.

3.4 CIRCULAR POLARIZATION MEASUREMENTS. RESULTS AND ANALYSIS. — 3.4.1 *Measurement of* θ. — We have defined θ by equation (11). It is easy to verify theoretically that $I_{\sigma^+}(B) = I_{\sigma^-}(-B)$. By

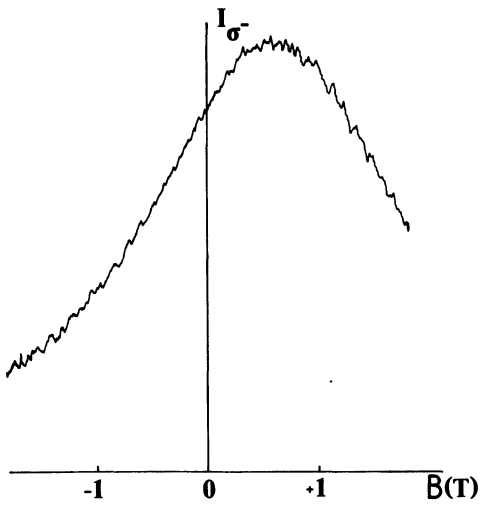

Fig. 6*b*. — Example of an experimental curve $I_{\sigma^-} = f(B)$ recorded for an R fluorescence line coming from the level $v'=21$ $J'=133$.

measuring I_{σ^-} for opposite values of the field B, one gets : $I_{\sigma^+}(B) - I_{\sigma^-}(B) = I_{\sigma^-}(-B) - I_{\sigma^-}(B)$; therefore θ is measured from a single curve, without any problem of calibration. The accuracy of the measurement of θ is limited by two factors :

— the signal to noise ratio. This error depends very much on the fluorescence intensity, i.e., on the level and on the iodine pressure ; its absolute value is usually of the order of 0.005 to 0.05 (θ varying in the range 0.03 to 0.5);

— the quality of the circular analyser ; by a thorough study of this apparatus, we have estimated this error to be less than $0.05 \times \theta$.

Usually, the first term dominates the second.

We shall now consider all the dependences of θ that we have studied, looking either for a confirmation of the theory or for a measurement of a predissociation parameter. In all experiments, θ_{RR} appears to be negative ; θ will designate in fact the modulus of θ. The fact that θ_{RR} is negative proves that α_v and C_v have the same sign.

3.4.2 *Variation of θ with the excitation beam polarization.* — This experiment was done with the Kr^+ laser. Table I gives a list of the levels studied, the values of θ_π and θ_σ for a given iodine pressure, and their ratio. As indicated by equation (13), the ratio θ_π/θ_σ should be in the range 0.48-0.62. This point is verified in table I.

Table I. — *θ_π and θ_σ for various levels excited by the Kr^+ laser.*

v'	17	18	21	40	
J'	36	95	116	77	
p (mtorr)	30	30	30	3	72
θ_σ	0.046	0.150	0.232	0.211	0.140
θ_π	0.021	0.085	0.129	0.117	0.083
θ_π/θ_σ	0.46	0.57	0.56	0.55	0.59

From now on, we will consider only measurements of θ_σ, designated for brevity by θ.

3.4.3 *Variation of θ with iodine pressure.* — Some systematic studies were made on the levels excited by the HeNe laser ($v = 6$ $J = 32$, $v = 11$ $J = 128$) and the following levels excited by the dye laser :

$$v = 10 \quad J = 70 \text{ and } 100$$
$$v = 11 \quad J = 70, 100, 115 .$$

We show in figure 7 the results of this study for the two levels $v = 10$ $J = 70$ and 100. It appears clearly that the decrease of θ with pressure is slow. For an iodine pressure of 150 mtorr, Γ_{coll} is almost equal to

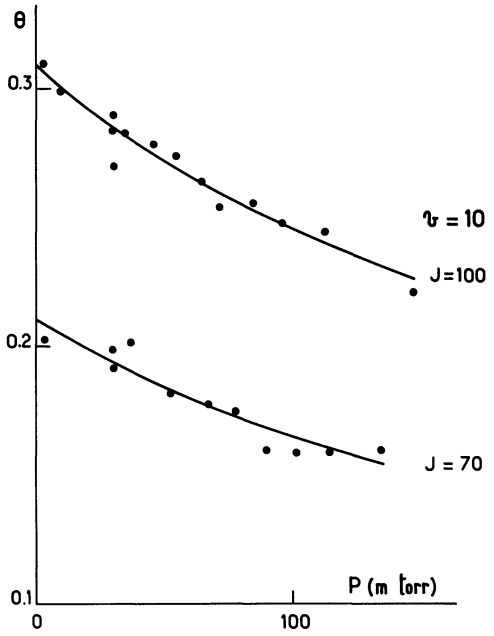

Fig. 7. — Plot of θ as a function of iodine pressure for the two levels $v' = 10$ $J' = 70$ and 100. The points are experimental and the curves represent the best fit obtained with the parameters given in table II.

three times Γ_{rad}, and θ is reduced from its zero pressure value by only 20-25 %. This is in good agreement with the saturation observed in figure 3*b* on the curve $\theta = f\left(\frac{C_{vJ}\,J}{\sqrt{\Gamma}}\right)$ when $y_J = a_{vJ}/(C_{vJ}\,J)$ is constant. Such a behaviour cannot be explained by the former theory [10], with reasonable values of the radiative and collisional decay rates, because in this theory there was no saturation of θ.

The curve of θ *vs.* iodine pressure depends on the combinations of parameters $C_{vJ}/\sqrt{\Gamma_{rad}}$, $a_{vJ}/\sqrt{\Gamma_{rad}}$, and σ/Γ_{rad}, where σ is the collisional cross-section. As Γ_{rad} [14] and σ [24, 25] are well known for the levels $v = 10$ and 11, we have fitted a theoretical curve to the experimental points by varying only C_{vJ}^2/Γ_{rad} and $Y^2 = a_{vJ}^2/C_{vJ}^2$ for the level $v = 10$.

For $v = 11$, where the sensitivity to Y^2 was weaker,

we fixed Y^2 to the value determined previously [14] (in both cases, Y was taken negative).

It is interesting to note the very good agreement between the theoretical curve and the experimental points on figure 7. Table II gives the values of the parameters providing the best fit. The value of Y^2 thus determined $Y^2 = 940 \pm 300$ and $Y^2 = 950 \pm 150$ are in acceptable agreement with the value determined in the previous paper [14] for the level $v = 10$

$$Y^2 = 1\,205 \pm 160$$

and the average value

$$Y^2 = 1\,120 \pm 160\,.$$

Similarly, the values of $C_{vJ}^2/\Gamma_{\text{rad}}$ are in agreement with the previous determinations of this quantity.

Table II. — *For each level in which θ has been studied as a function of the pressure, we give in this table the quantum numbers of the level, the value of the ratio $\sigma/\Gamma_{\text{rad}}$, the value of $Y^2 = a_{vJ}^2/C_{vJ}^2$, and the value of $C_{vJ}^2/\Gamma_{\text{rad}}$. An asterisk indicates that the corresponding parameter was fixed at this value during the fit.*

v'	J'	$10^4\ \sigma/\Gamma_{\text{rad}}$	Y^2	$10^6\ \frac{C_{vJ}^2}{\Gamma_{\text{rad}}}$
—	—	—	—	—
10	70	0.88 *	940	143
			± 300	± 45
10	100	0.88 *	950	174
			± 150	± 40
11	70	0.93 *	1 120*	116
				± 22
11	100	0.93 *	1 120*	155
				± 15
11	115	0.93 *	1 120*	140
				± 33
11	128	0.93 *	1 120*	133
				± 30

3.4.4 *Variation of θ with the rotational and vibrational quantum numbers.* — θ has been measured on 146 rovibrational levels, almost always for an iodine pressure of 30 mtorr. It is not possible to give all these results here, but we are going to illustrate the most important behaviour, i.e. the variation of θ with J and v.

a) Variation of θ with the rotational quantum number J. — Figure 8 shows the variation of θ with J for some vibrational levels. In the common case illustrated by the levels $v = 9$ and 21, θ is, to a good approximation, a linear function of J. This is in agreement with the calculations illustrated in figure 3. However, the strong curvatures of the plots for the levels $v = 12$ and 16, in figure 8, is simply due to the variation with J of the Franck-Condon density for predissociation. This relative variation is not very large for the levels $v = 9$ and 21, thus the plots are linear. For $v = 12$ the Franck-Condon density increases with J, which explains the upward curvature of the corresponding plot of θ *vs.* J, $v = 16$ and also, but less strikingly, $v = 18$ exhibit the opposite behaviour.

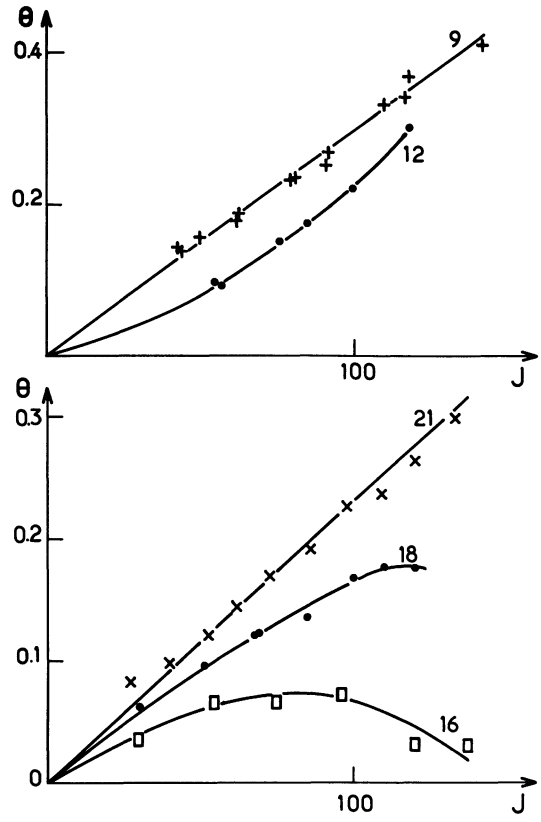

Fig. 8. — Plot of θ as a function of J for the levels $v' = 9$, 12 and $v' = 16$, 18, 21. Note the different vertical scales for the two sets of levels. The scatter of the points gives an idea of the experimental error and the curves are just rough interpolations of the data.

The calculation of θ depends, for a fixed rovibrational level vJ, on the values of C_{vJ}^2/Γ and $Y^2 = a_{vJ}^2/C_{vJ}^2$, and on the hyperfine structure of the line, which determines the coefficients $\alpha(I\varepsilon JF)$ and the weight factors $w_{\varepsilon F}$. As the hyperfine parameters are well known [26], by fixing Y^2 to the average value determined in the previous paper [14] ($Y^2 = 1\,120$, $Y < 0$) we can determine from θ the value of C_{vJ}^2/Γ. We have plotted the values thus determined as a function of $J(J + 1)$ in figure 9. For each vibrational level, we have also plotted the theoretical J dependence

$$\frac{C_{vJ}^2}{\Gamma} = \frac{C_v^2}{\Gamma}(1 + p_v J(J + 1) + q_v[J(J + 1)]^2) \quad (18)$$

in which only C_v^2/Γ was fitted while p_v and q_v were fixed to their calculated values [14]. It appears that this theoretical dependence is in good agreement with the experimentally observed variation of C_{vJ}^2/Γ. However, the experimental points are not very precise : this low precision is due to the fact that θ is linear in $C_{vJ}\,J/\sqrt{\Gamma}$ for small values of this quantity. This type of relation implies a very high sensitivity to C_{vJ}^2/Γ but a doubled relative error. Moreover, the linearity

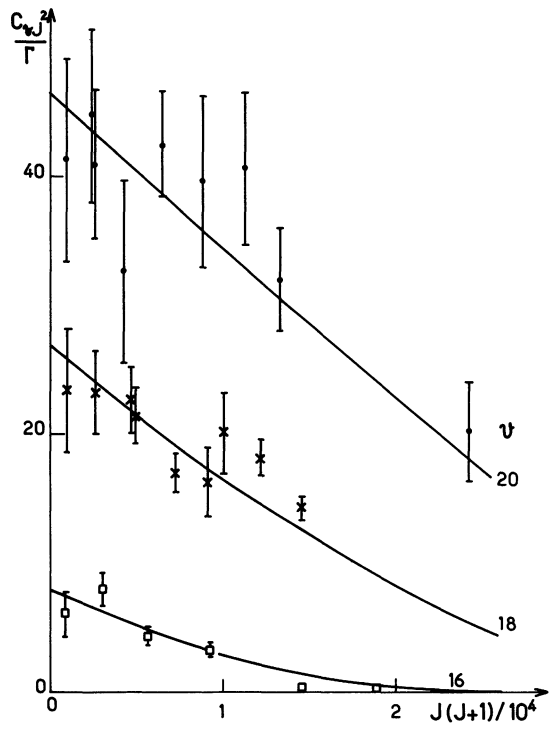

Fig. 9. — Plot of the values of C^2_{vJ}/Γ as a function of $J(J+1)$, for the levels $v = 16$, 18, 20. The points are experimental and the full curves represent the corresponding calculated J-variation.

of θ in J implies that the relative error is very large for small J values.

In table III we give the values of C_v^2/Γ extracted from these fits and their error bars. It appears that the results are rather precise for $9 \leqslant v \leqslant 22$. For $v < 9$ the error increases very rapidly and the values obtained are meaningless; only a lower bound is

Table III. — *We give, for all the vibrational levels studied, the value of* $C_v^2/(\Gamma_{rad} + \Gamma_{coll})$ *obtained by the least square fit described in the text. The collisional decay rate* Γ_{coll} *corresponds to a pressure of* 30 mtorr.

v	$10^6\ C_v^2/(\Gamma_{rad}+\Gamma_{coll})$	v	$10^6\ C_v^2/(\Gamma_{rad}+\Gamma_{coll})$
6	> 120	16	8 ± 2.4
7	> 65	17	18 ± 6
8	> 120	18	27 ± 3
9	135 ± 40	19	35 ± 4.5
10	107 ± 30	20	47 ± 6
11	43 ± 8	21	55 ± 8
12	20 ± 7	22	59 ± 16
13	2.6 ± 0.2	24-27	76 ± 19
14	not measured	28-29	75 ± 30
15	0.7 ± 0.7	30-34	55 ± 30
		35-37	43 ± 12

given for the levels $v = 6$, 7, 8. For $24 \leqslant v \leqslant 37$, the number of measurements is small and their precision is not very good. We have combined data from several consecutive vibrational levels to perform this study.

b) Variation of θ with the vibrational quantum number. — Figure 10 shows the variation of θ with v. The value of θ is taken for $J = 100$ (obtained by interpolation of plots of the type appearing in figure 8). This figure shows clearly the very rapid variation of θ around $v = 14$. Near $v = 14$, C_v^2 passes through a minimum equal to zero, but θ behaves like $|C_v|$, as theoretically predicted.

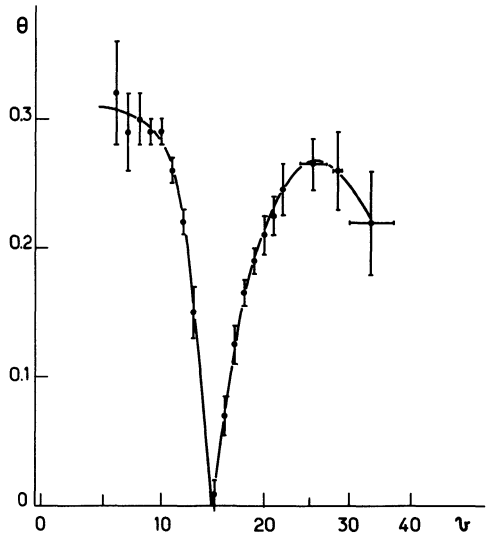

Fig. 10. — Plot of the vibrational variation of θ (interpolated to $J = 100$). The horizontal scale is linear in vibrational energy, and the presence of an horizontal error bar indicates that the J interpolation has been made on a group of vibrational levels. The full curve is a rough interpolation of the points.

Another interesting point is the saturation of θ near $v = 6$; although $C_7^2/C_{10}^2 \approx 3$ (see table 1 of reference [14]) the variation of θ between $v = 6$ or 7 and $v = 10$ is extremely small, as indicated by table IV.

Table IV. — *This table contains the value of* θ *for* $J = 100$ *obtained by an interpolation of the plots represented on figure* 8.

v	θ	v	θ
6	0.32 ± 0.040	16	0.07 ± 0.015
7	0.29 ± 0.030	17	0.125 ± 0.015
8	0.30 ± 0.020	18	0.165 ± 0.010
9	0.29 ± 0.010	19	0.190 ± 0.010
10	0.29 ± 0.010	20	0.21 ± 0.015
11	0.26 ± 0.010	21	0.225 ± 0.015
12	0.22 ± 0.010	22	0.245 ± 0.020
13	0.15 ± 0.020	24-27	0.265 ± 0.020
14	not measured	28-29	0.260 ± 0.030
15	0.01 ± 0.010	30-37	0.22 ± 0.040

If we suppose that for all these levels, $Y^2 = a_v^2/C_v^2$ is exactly constant, this behaviour implies that θ has reached the saturation plateau in the curve $\theta = f\left(\frac{C_v J}{\sqrt{\Gamma}}\right)$ at constant y_J (see Fig. 3*b*). From the

content of table IV, we determine the saturation value of θ for $J = 100$

$$\theta_{sat} = 0.31 \pm 0.02 .$$

This saturation value depends only on $y_J = Y/J$. In figure 11 we have plotted the theoretical curve $\theta_{sat} = f(y_J)$. By intersecting this curve with the observed value of θ_{sat}, we get a determination of y_J and hence a new determination of Y^2

$$Y^2 = 1\,180 \pm 120 .$$

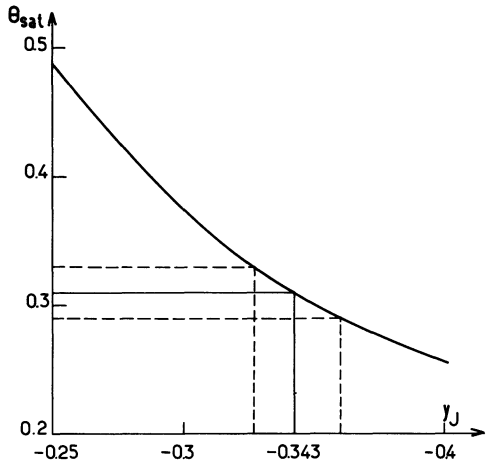

Fig. 11. — Graphical determination of $y_J = a_{vJ}/C_{vJ}$ J from the observed value of $\theta_{sat} = 0.31 \pm 0.02$. The full curve represents the calculated variation of θ_{sat} with y_J.

This value is in very good agreement with the determination in the previous paper [14], $Y^2 = 1\,120 \pm 160$.

From this discussion it is now very clear that for $v = 6, 7, 8$, the knowledge of θ can give only a lower bound on C_v^2/Γ_{rad} as θ is saturated. This explains the difficulties encountered in paragraph 3.4.4.*a*).

3.4.5 *Values of* C_v^2 *and* Γ_{rad}. — We know now $C_v^2/(\Gamma_{rad} + \Gamma_{coll})$ (Γ_{coll} corresponding to 30 mtorr of iodine) and we have confirmed the value of Y^2 by two new determinations.

It is possible to extract C_v^2 and Γ_{rad} if we know the total decay rate Γ_{tot} at zero pressure and the collision cross-section. We may use the measurements of Broyer *et al.* [25], Paisner *et al.* [27] and Shotton *et al.* [28]. Although numerous measurements due to Capelle *et al.* [24] are available, as the excitation was not selective, the decay rates are averaged over many levels and we do not use them in the following.

For vibrational levels $v > 22$ only a very small number of measurements are available. Table V presents a summary of the measurements of Paisner *et al.* [27] and our unpublished values [18, 12, 21]. Using those measurements, we determine Γ_{rad} for $v = 32, 40, 43$. Those values are used for determining an interpolation formula, which will be discussed in part 4. Table VI presents all the available values of Γ_{rad} and C_v^2. When a first determination of Γ_{rad} and C_v^2 appears in reference [14], the present value is an average of the two measurements. For the level $v = 43$ we have used the value [14] of a_v^2/Γ_{rad} to calculate Γ_{rad} from Γ_{tot}; for $v = 62$ and 70, we suppose that the predissociation is very small and we feel that Γ_{rad} is very close to Γ_{tot}; surely Γ_{rad} is smaller than Γ_{tot} and this explains the inequalities appearing in table VI. The curves Γ_{rad} and C_v^2 as a function of v appear in section 4 of the present paper.

Table V. — *Summary of the values of the total decay rate* Γ_{tot} *for the levels excited by the* Ar^+ *and* Kr^+ *lasers.*

v	J	Γ_{tot} (10^6 s^{-1}) Reference [27]	Γ_{tot} (10^6 s^{-1}) Our work
21	116	1.45 ± 0.04	1.82 ± 0.65
32	9 and 14	0.92 ± 0.03	0.94 ± 0.13
40	77	0.70 ± 0.02	0.62 ± 0.10
43	12 and 16	0.44 ± 0.02	0.43 ± 0.12
62	27	0.11 ± 0.02	0.083 ± 0.014
70	55	not measured	0.038 ± 0.012

Table VI. — *Values of* Γ_{rad} *and* C_v^2 *for all vibrational levels studied. No measurement of* C_v^2 *is available for* $v < 7$ *or* $v > 40$. *Although we give for* Γ_{rad} *only an upper limit equal to* Γ_{tot} *for* $v = 62$ *and* 70, *we believe that* Γ_{rad} *and* Γ_{tot} *are very similar for these levels. The values of* $\Gamma_{rad}(v)$ *with an asterisk are obtained by interpolation* (*see* § 4.3).

v	Γ_{rad} 10^6 s^{-1}	C_v^2 s^{-1}	v	Γ_{rad} 10^6 s^{-1}	C_v^2 s^{-1}
7	1.05 (9)	287 (21)	19	0.68 (8)	42 (5)
8	0.95 (8)	187 (13)	20	0.73 (10)	55 (7)
9	0.97 (6)	141 (6)	21	0.70 (25)	64 (9)
10	0.78 (9)	95 (7)	22	0.65 *	69 (15)
11	0.75 (10)	51 (7)	24-27	0.61 *	80 (20)
12	0.74 (9)	21 (8)	28-29	0.55 *	74 (30)
13	0.78 (6)	3.0 (0.5)	30-34	0.50 *	52 (28)
14	0.76 (3)	< 2	35-37	0.44 *	38 (10)
15	0.72 (7)	1 (1)	40	0.38 (10)	26 (10)
16	0.73 (7)	9 (3)	43	0.35 (5)	
17	0.74 (5)	23 (6)	62	$\lesssim$ 0.08 (1)	
18	0.78 (6)	33 (4)	70	$\lesssim$ 0.04 (1)	

3.5 THE TOTAL FLUORESCENCE INTENSITY CURVES AND THEIR ANALYSIS. — On all the levels that were studied, at least one curve $\mathfrak{I} = I_{\sigma^+} + I_{\sigma^-} = f(B)$ was recorded, usually for an iodine pressure of 30 mtorr. We are going to discuss the information deduced from these curves.

3.5.1 *Shape of the curve* $\mathfrak{I} = f(B)$. — We have noted that these curves were not of Lorentzian shape as soon as the gyroscopic predissociation rate was comparable with $\Gamma = \Gamma_{rad} + \Gamma_{coll}$. This is, for instance, the case for the level $v = 11$ $J = 128$ excited by the HeNe laser. However, we wanted to verify the existence of a maximum of intensity at a nonzero magnetic field. As shown in figure 5, this demands a very high J value and a high predissociation rate.

This was achieved for the level $v = 10$ $J = 161$; the corresponding curve $\mathfrak{I} = f(B)$ is plotted in figure 12 and clearly shows an intensity maximum at a non-zero field. The dotted curve represents a best fit to the experimental data.

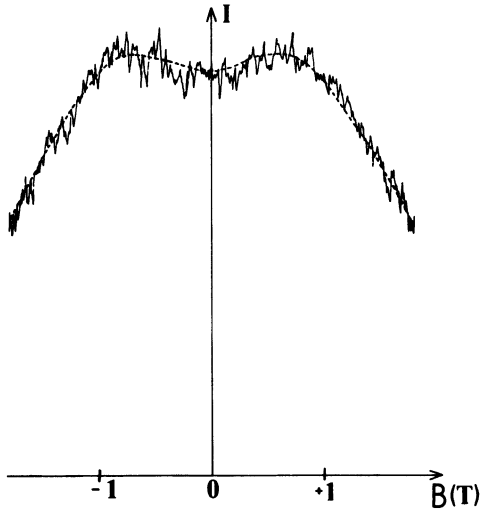

Fig. 12. — Total fluorescence intensity as a function of the magnetic field recorded for the level $v' = 10$ $J' = 161$ (with an iodine pressure $p = 30$ mtorr). The full curve is experimental and the dotted curve is the best fit. The presence of an intensity maximum at nonzero field is clear.

This is a definite proof of a previously unobserved effect. The very high J values necessary to observe it and the weakness of the effect explain why it was not observed before [5, 6]. More precisely, in the experiments of reference [5], the excitation was not selective and the observed curves were averages over many levels; in such averages, the high J levels have always a very small weight. For the experiments of reference [6], the study of the level $v = 11$ $J = 128$ should have shown a slight deviation from a Lorentz curve; but the signal to noise ratio was no sufficient to detect this deviation.

3.5.2 *Some qualitative observations.* — In the general case, the curve $\mathfrak{I} = f(B)$ is not Lorentzian and it is difficult to extract from this curve a single parameter. However, near $v = 14$, the predissociation coefficients are small and we are, more or less, in the conditions of validity of equation (15). As α_v is small, only the top of the curve is observed and it is easy to calculate an apparent $b_{vJ}/(\Gamma_{\text{rad}} + \Gamma_{\text{coll}})$. The measured values of this parameter are plotted in figure 13 as a function of $J(J + 1)$ for the levels $v \doteq 14, 15, 16$. To enable comparison, the theoretical *FCD* variation is also plotted. It is clear that b_{vJ}/Γ and the *FCD* are not far from proportional; the deviation occurring for $v = 16$ is probably due to the invalidity of equation (15) for this level which displays a non-negligible predissociation.

We are now going to present an analysis of all $\mathfrak{I} = f(B)$ curves using a least squares method. The

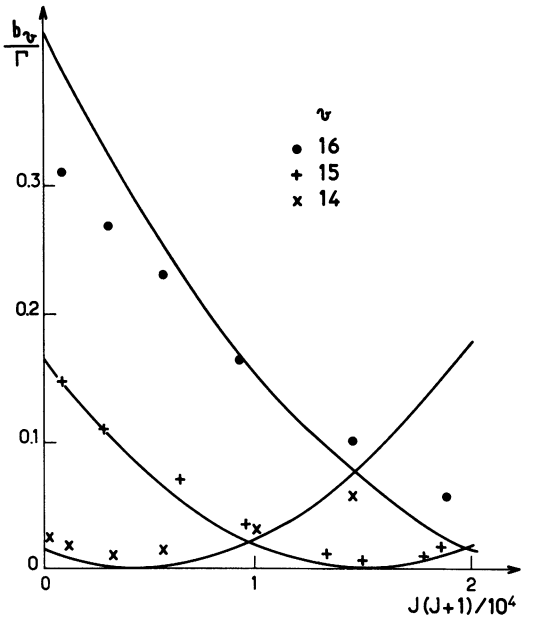

Fig. 13. — This figure represents the experimental parameter b_{vJ}/Γ as a function of $J(J + 1)$ for the levels $v = 14, 15, 16$. The full curves are proportional to the calculated Franck-Condon density (same proportionality factor for the three curves).

results presented above have the advantage of being direct experimental results which are insensitive to any error in the parameters used in the fits.

3.5.3 *Measurement of* α_{vJ}^2. — We already know Γ_{rad}, Γ_{coll}, C_v^2, a_v^2 and their theoretical J dependence given by p_v, q_v. We can deduce the parameter α_{vJ}^2 from a fit of the curve $\mathfrak{I} = I_{\sigma^+} + I_{\sigma^-} = f(B)$. This is the fit that was used for figure 12.

In practice, Γ_{rad} and C_v^2 are taken from table VI. The theoretical values of p_v and q_v are used [14]. Y^2 is held fixed at 1 120 ($Y < 0$). The collision cross-section is taken equal to 70 Å^2 for $v < 13$ and 65 Å^2 for $v \geqslant 13$. On each curve 11 points were measured and the only parameter fitted was α_{vJ}^2.

The values obtained for α_{vJ}^2 for one vibrational level were then fitted to their theoretical J dependence

$$\alpha_{vJ}^2 = \alpha_v^2[1 + p_v J(J + 1) + q_v[J(J + 1)]^2] \quad (19)$$

by varying only α_v^2.

In figure 14 we show a plot of α_{vJ}^2 as a function of $J(J + 1)$ for several vibrational levels. The agreement between the theoretical and observed J dependence is very good.

We give in table VII the values of α_v^2 extracted from the fit. As no value of C_v^2 was available for $v = 4, 5, 6$, we have fixed the ratio $Z^2 = \alpha_{vJ}^2/C_{vJ}^2$ to the average value measured on $v = 7$ and 8

$$Z^2 = 0.505 \times 10^5 .$$

The quality of the experimental data is high, and therefore the errors are small. The error bars in table VII include the statistical effects on α_{vJ}^2 resulting from

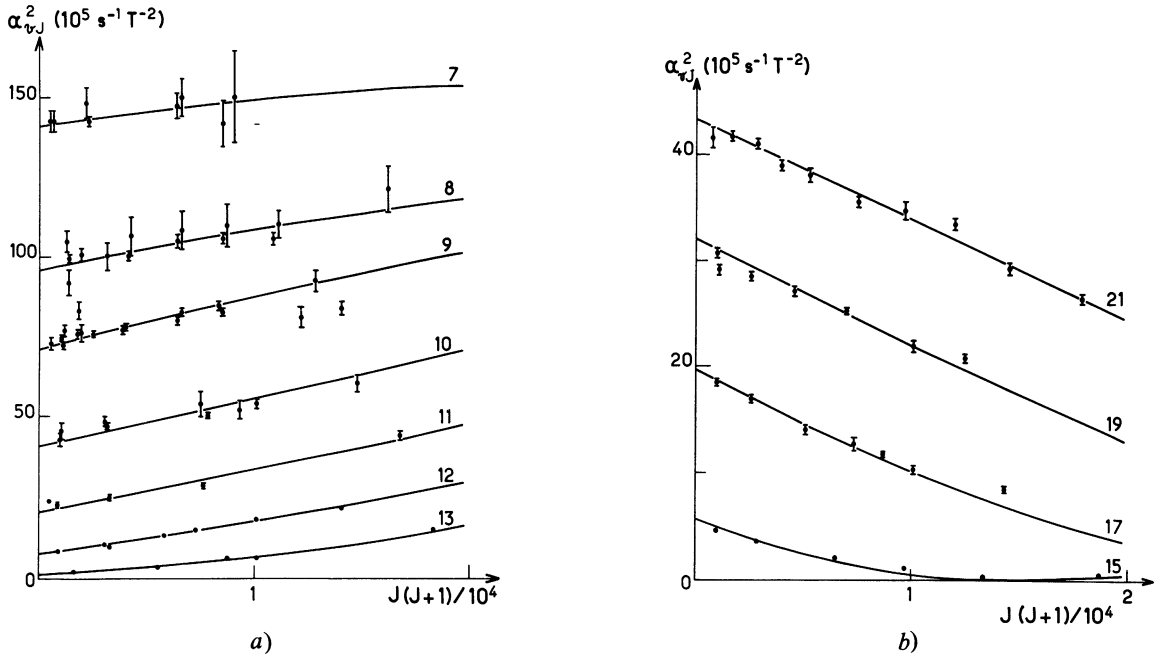

Fig. 14*a* and *b*. — Plots of the measured values of α^2_{vJ} as a function of $J(J+1)$ for the levels $v' = 7, 8, 9, 10, 11, 12, 13$ and $v' = 15, 17, 19, 21$. The high quality of the data is shown by the small scatter of the points, and the agreement with the calculated J-variation of the Franck-Condon density is striking. Where not apparent, the error bar is smaller than the size of the points.

Table VII. — *Summary of all the values of α^2_v obtained by the study of the curves $\mathfrak{I} = I_{\sigma^+} + I_{\sigma^-} = f(B)$. The error bars do not take into account the uncertainties in Γ_{rad} and in the other predissociation parameters.*

v	$\alpha^2_v/10^5$ s^{-1} T^{-2}	v	$\alpha^2_v/10^5$ s^{-1} T^{-2}
4	154 ± 33	16	13.8 ± 2.4
5	174 ± 10	17	19.8 ± 1.1
6	173 ± 20	18	28.5 ± 1.2
7	141 ± 2	19	32.2 ± 1.8
8	96 ± 3	20	39.3 ± 1.8
9	71 ± 2	21	43.3 ± 0.8
10	41 ± 1	22	44.6 ± 1.5
11	20.8 ± 2	24-27	44.6 ± 1.2
12	7.8 ± 0.4	28-29	41.3 ± 2.5
13	1.10 ± 0.12	30-34	28.3 ± 3.6
14	0.54 ± 0.01	35-39	20.7 ± 3.6
15	5.70 ± 0.70		

Table VIII. — *Values of a_v^2 deduced from the measurement of a_v^2/Γ_{rad} (reference [14]) and the present determination of $\Gamma_{rad}(v)$ (Table VI).*

v	a_v^2 (10^3 s^{-1})	v	a_v^2 (10^3 s^{-1})
7	324 ± 26	16	23 ± 8
8	232 ± 18	17	37 ± 5
9	146 ± 12	18	51 ± 8
10	110 ± 17	19	61 ± 12
11	40 ± 15	20	67 ± 20
12	16 ± 5	21	88 ± 50
13	3 ± 3	22	88 ± 30
14	4 ± 10 4		
15	13 ± 13	43	12 ± 5

the noise in the curves, but no account is made for the errors in all parameters introduced in the fit.

4. **Interpretation of the results.** — 4.1 SUMMARY OF THE VARIATIONS OF THE PREDISSOCIATION PARAMETERS. — Tables VI and VII give our best values of Γ_{rad}, C_v^2, α_v^2 as functions of v. In table VIII we present the best values of a_v^2 deduced from the measurements of reference [14] and from the values of Γ_{rad} (Table VI).

In figures 15, 16, 17 we have plotted the vibrational variation of C_v^2, a_v^2, α_v^2. In each case, we have tried to represent the observed variation of the parameter by the product of the calculated Franck-Condon density [14] and a scaling factor. The resulting values of the scaling factors are given in the following equations :

$$C_v^2 = (5.8 \pm 1).10^5 \; FCD(v)$$
$$a_v^2 = (6.7 \pm 0.6).10^8 \; FCD(v)$$
$$\alpha_v^2 = (3.1 \pm 0.2).10^{10} \; FCD(v) \qquad (20)$$

where C_v^2 and a_v^2 are measured in s^{-1}, α_v^2 in s^{-1} T^{-2} and the FCD in cm.

The first comment is that the agreement between the experimental points and the calculated curves is extremely good for α_v^2 and a_v^2. It is less satisfactory for C_v^2. This disagreement for C_v^2 is probably due to a violation of the Franck-Condon approximation due to a rapid dependence of the corresponding electronic matrix element on the internuclear distance. The

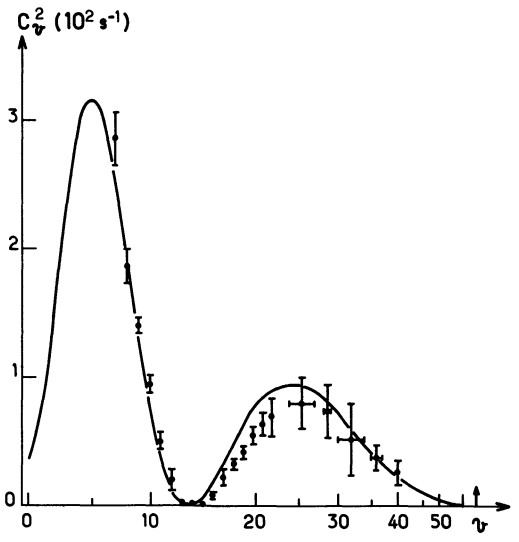

Fig. 15. — Plot of the values of C_v^2 (for $J = 0$) measured on the levels $v' = 7$-40. The equation for the curve is

$$C_v^2 = 5.8 \times 10^5 \, FCD(v) .$$

The vertical arrow designates the dissociation limit and the horizontal scale is linear in vibrational energy (also true for the figures 16, 17, 18).

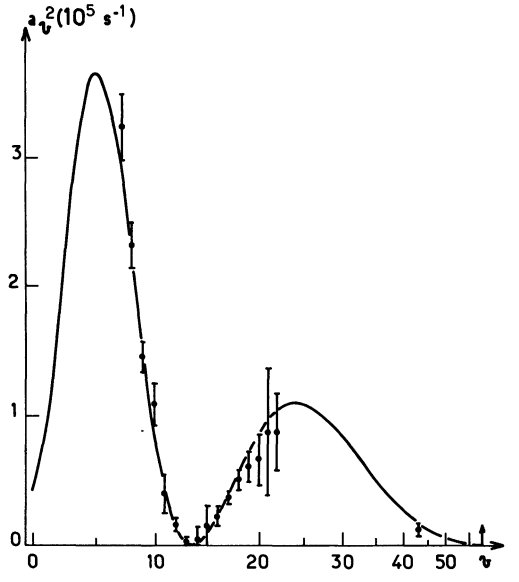

Fig. 16. — Plot of the values of a_v^2 (for $J = 0$) measured for the levels $v' = 7$-22 and $v' = 43$. The equation for the curve is

$$a_v^2 = 6.7 \times 10^8 \, FCD(v) .$$

quality of the agreement for α_v^2 and a_v^2 means that the Chapman and Bunker [6] potential curve for the 1_u state is very precise, provided that our semiclassical calculation of the *FCD* introduces a negligible error. From the values of the proportionality coefficients between C_v^2, a_v^2, α_v^2 and the Franck-Condon density, we can easily deduce the electronic matrix elements. We use the definitions appearing in the first paper of this series [13]. We need only convert the *FCD* into

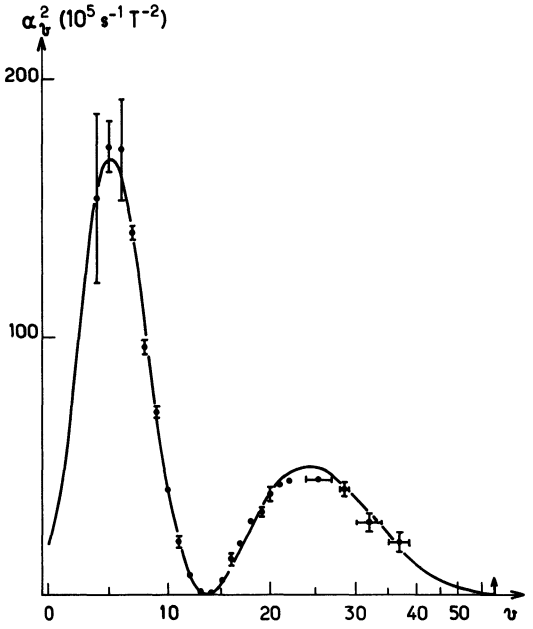

Fig. 17. — Plot of the values of α_v^2 (for $J = 0$) measured for the levels $v' = 4$-39. Where not apparent, the error bar is smaller than the size of the point. The equation for the curve is

$$\alpha_v^2 = 3.1 \times 10^{10} \, FCD(v) .$$

an inverse energy unit (*FCD* (cm) = 10^2 *hcFCD* (joule^{-1})).

The absolute sign of a matrix element is meaningless, but relative signs do matter. We know that a_v and C_v are of opposite signs, and from the sense of the circular polarization, we have deduced that C_v and α_v are of the same sign. Table IX summarizes the results.

Table IX. — *Electronic matrix elements deduced from the predissociation parameters* ($|\varepsilon|^2 = 1$).

Parameter	Corresponding electronic matrix element
C_v	$\langle 0^+ \, u \mid \overline{T^1_{-1}(L) + T^1_{-1}(S)} \mid 1_u \rangle = +(0.015\,6 \pm 0.001\,3)\,\varepsilon$
a_v	$\dfrac{f_1(a, 1_u, 0^+ u)}{[I_a(I_a+1)(2I_a+1)]^{1/2}} = -(0.713 \pm 0.030).10^9 \, \varepsilon$ Hz
α_v	$\langle 0^+ \, u \mid \overline{T^1_{-1}(L) + 2\,T^1_{-1}(S)} \mid 1_u \rangle = -(0.347 \pm 0.011)\,\varepsilon$

The most striking point is that the matrix elements of **L** and **S** cancel each other almost perfectly in C_v; by combining the equations for C_v and for α_v; we get :

$$\langle 0^+ \, u \mid T^1_{-1}(L) \mid 1_u \rangle = \quad 0.378 \, \varepsilon$$

$$\langle 0^+ \, u \mid T^1_{-1}(S) \mid 1_u \rangle = -\, 0.363 \, \varepsilon$$

where $|\varepsilon|^2 = 1$.

These two matrix elements are almost equal in modulus, but their algebraic sum is less than 1/20 of each term. This point is partly explained in section 4.2. A consequence of this property is that even if the L and S matrix elements vary slowly with the internuclear distance r, their algebraic sum may vary much more rapidly with r; this should explain the previously

invoked violation of the Franck-Condon approximation for C_v^2, whereas no such violation should exist for α_v^2 or a_v^2, because the corresponding matrix elements are not small.

4.2 AN APPROXIMATE THEORY OF THE ELECTRONIC MATRIX ELEMENT. — One can try to calculate the electronic matrix elements. It is difficult to do an *ab initio* calculation on I_2 (106 electrons !), although some calculations of this type have been made [34].

We present the following two calculations. In the first one, the molecular wavefunctions are taken as pure states in a case a basis, which can only be an extremely rough approximation for I_2. In the second calculation, the molecular wavefunctions are written in the separated atom approximation [29], which is certainly a very good approximation for large internuclear distances [30], but should be rather poor here (as the B-1_u potential curve crossing occurs at $r \approx 2.89$ Å).

In the case a basis set, the B state is a $^3\Pi_{0^+u}$, the 1_u state is a $^1\Pi_{1u}$. Due to the singlet character of the 1_u state and the triplet character of the B state, the matrix elements for C_v and α_v vanish. The quadrupolar hyperfine term (neglected throughout these papers) vanishes too, while the magnetic dipole hyperfine term is the only one different from zero; its evaluation would demand that we write out a detailed wavefunction (for instance LCAO-MO).

In the separated atom approximation, we specify the wavefunction corresponding to an infinite internuclear distance, which is simply the correctly symmetrized product of atomic wavefunctions. For the B state

$$|\,0^+\,u\,\rangle = \tfrac{1}{2}[|\,\tfrac{3}{2},\tfrac{1}{2}\,\rangle_a\,|\,\tfrac{1}{2},-\tfrac{1}{2}\,\rangle_b + |\,\tfrac{1}{2},-\tfrac{1}{2}\,\rangle_a\,|\,\tfrac{3}{2},\tfrac{1}{2}\,\rangle_b + |\,\tfrac{3}{2},-\tfrac{1}{2}\,\rangle_a\,|\,\tfrac{1}{2},\tfrac{1}{2}\,\rangle_b + |\,\tfrac{1}{2},\tfrac{1}{2}\,\rangle_a\,|\,\tfrac{3}{2},-\tfrac{1}{2}\,\rangle_b] \quad (21)$$

where $|\,j, m_j\,\rangle_x$ designates the wavefunction of the atom $x\,|\,^2P_j, m_j\,\rangle$ with the internuclear axis as the quantization axis.

Two 1_u states arise from the ground state dissociation limit (two $^2P_{3/2}$ atoms). It is not clear which one or which linear combination is the 1_u state considered here :

$$|\,1_u\,\rangle_\alpha = |\,\tfrac{3}{2},\tfrac{1}{2}\,\rangle_a\,|\,\tfrac{3}{2},\tfrac{1}{2}\,\rangle_b$$

$$|\,1_u\,\rangle_\beta = \frac{1}{\sqrt{2}}[|\,\tfrac{3}{2},\tfrac{3}{2}\,\rangle_a\,|\,\tfrac{3}{2},-\tfrac{1}{2}\,\rangle_b + |\,\tfrac{3}{2},-\tfrac{1}{2}\,\rangle_a\,|\,\tfrac{3}{2},\tfrac{3}{2}\,\rangle_b]\,. \quad (22)$$

It is easy to calculate the matrix elements for the various terms, using the atomic matrix elements and following the principles developed in references [12, 30]. In table X we give the results of these calculations for the two wavefunctions $|\,1_u\,\rangle_\alpha$, $|\,1_u\,\rangle_\beta$.

Among the positive results, it appears that in both cases there is a perfect cancellation of the L and S term in the C_v matrix element : this is simply due to the fact that $\mathbf{L} + \mathbf{S} = \mathbf{j}_a + \mathbf{j}_b$ and clearly $T^1_{-1}(j_x)$ cannot change j_x from 1/2 to 3/2. Moreover, the matrix elements of $\mathbf{L}$ and $\mathbf{S}$ are not zero and the matrix element for α_v is not zero either. We see that this separated atom basis gives a nice account of the weakness of the gyroscopic term C_v. Unfortunately the agreement is not very good for the other matrix elements. In the general case, the 1_u wavefunction is a linear combination of $|\,1_u\,\rangle_\alpha$ and $|\,1_u\,\rangle_\beta$ (namely

$$|\,1_u\,\rangle = \cos\phi\,|\,1_u\,\rangle_\alpha + \sin\phi\,|\,1_u\,\rangle_\beta)\,.$$

It is easy to verify that the theoretical ratio of matrix elements for a_v and α_v is independent of ϕ and equal to − 407 MHz in disagreement of magnitude and sign with the experimental value of + 2 050 MHz. Finally, the hyperfine quadrupolar term, although dependent on ϕ, seems large and its effect should have been observed.

Table X. — *This table gives the values of the four predissociation matrix elements using the separated atom approximations of the wavefunctions* $|\,1_u\,\rangle_\alpha$, $|\,1_u\,\rangle_\beta$ *and states the selection rules for the pure case a wavefunction* ($I_a = 5/2$).

Matrix element \ Wavefunction of the 1_u state	Case a $^1\Pi_{1u}$	$\|\,1_u\,\rangle_\alpha$	$\|\,1_u\,\rangle_\beta$
$\langle\,0^+\,u\,\|\,T^1_{-1}(L)+T^1_{-1}(S)\,\|\,1_u\,\rangle$	0	0	0
$\langle\,0^+\,u\,\|\,T^1_{-1}(L)+2\,T^1_{-1}(S)\,\|\,1_u\,\rangle$	0	− 0.47	− 0.58
$\dfrac{f_1(a,\,1_u,\,0^+\,u)}{[I_a(I_a+1)\,(2\,I_a+1)]^{1/2}}$	≠ 0	192 MHz	235 MHz
$\dfrac{f_2(a,\,1_u,\,0^+\,u)\,[2\,I_a(2\,I_a-1)]^{1/2}}{[(2\,I_a+1)\,(2\,I_a+2)\,(2\,I_a+3)]^{1/2}}$	0	− 351 MHz	143 MHz

We see therefore that neither of the two approximate 1_u functions is very satisfactory. It appears also that we cannot really conclude anything about the importance of the quadrupolar hyperfine term; theoretically its magnitude is not known. However experimentally we may give some proof of its weakness :

— the experiments measuring a_v^2 give the same results (or results having a smooth v dependence) when they measure an average predissociation for one rotational level (e.g. non exponential decay) or when they test a few hyperfine sublevels (intensity measurement in a molecular beam);

— if an important predissociation term has been neglected, it should appear more or less in Γ_{rad} (as was the case when hyperfine predissociation was ignored [25, 11]); the resulting $\Gamma_{rad}(v)$ does not display any strong oscillation similar to the *FCD* for predissociation.

4.3 VARIATION OF THE RADIATIVE DECAY RATE $\Gamma_{rad}(v)$ AND INTERPRETATION. — In figure 18, we have plotted the values of $\Gamma_{rad}(v)$ which appear in table VII. Γ_{rad} decreases rapidly with the vibrational quantum number v and tends toward zero at the dissociation limit. This is well explained by the fact that, near the dissociation limit, most of the time, the molecule looks like two separated atoms for which the radiative decay is forbidden. (The B state dissociates into $^2P_{1/2} + {}^2P_{3/2}$ atoms ; all the lower states dissociate into $^2P_{3/2} + {}^2P_{3/2}$.

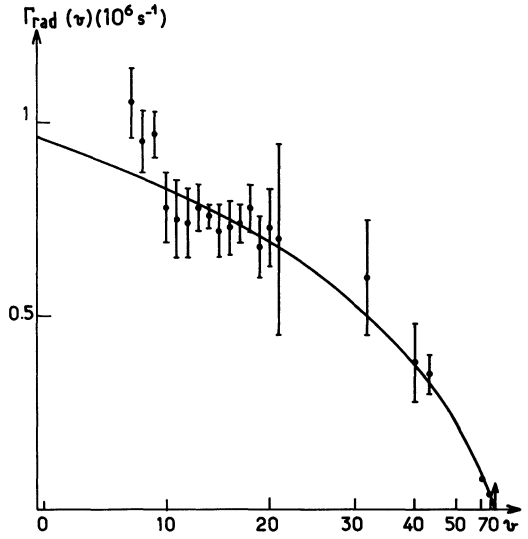

Fig. 18. — Plots of the values of Γ_{rad} measured for the vibrational levels $v' = 7$-22 and $v' = 32$, 40, 43, 62, 70. The curve represents equation (26) which is a semitheoretical calculation of $\Gamma_{rad}(v)$.

The $^2P_{1/2} \rightarrow {}^2P_{3/2}$ radiative transition is electric dipole forbidden because of parity.) Using a method described in [12, 30] we find that near the dissociation limit the radiative decay rate is given by :

$$\Gamma_{rad}(v) = P_1\, \gamma_{rad}(r_1) + P_2\, \gamma_{rad}(r_2), \qquad (23)$$

where r_1 and r_2 are the two turning points of the classical motion in the B state potential at the energy of level v ; P_1 and P_2 are the weights given to r_1 and r_2. Under the assumption that the vibrational anharmonicity is mainly due to the outer wing of the potential we get

$$P_1 = \omega_v/2\,\omega_e \qquad P_2 = 1 - P_1 \qquad (24)$$

where $\omega_v = \delta G(v)/\delta v$.

$\gamma_{rad}(r)$ is the radiative decay rate calculated for the molecule with fixed internuclear distance r. Using well known formulae and the assumption that the decay is mainly due to the B $\rightarrow$ X transition we get

$$\gamma_{rad}(r) = \frac{64\,\pi^4}{3\,h}\,[U_B(r) - U_X(r)]^3\,|\,D_{BX}(r)\,|^2 \qquad (25)$$

$D_{BX}(r)$ is the electric dipole for the B-X transition and its value is rather well known [31, 32, 35]. $U_B(r)$ and $U_X(r)$ are the potential curves of the B and X states. The behaviour of the quantity

$$|\,D_{BX}(r)\,|^2\,(U_B(r) - U_X(r))^3$$

is not simple ; for low values of r ($2.6 < r < 2.8$ Å), it is more a less constant because of a compensation of the increase of $D_{BX}(r)$ with r and a decrease of $(U_B(r) - U_X(r))$; then when r is in the range 2.8 Å-4 Å, $|\,D_{BX}(r)\,|^2$ and $(U_B(r) - U_X(r))^3$ are both decreasing and their product is rapidly decreasing. Finally for large r values $|\,D_{BX}(r)\,|^2$ should tend toward zero and $U_B(r) - U_X(r)$ should reach the limiting atomic value. From these considerations, it appears that if r is larger than 3.5-4 Å, $\gamma_{rad}(r)$ becomes negligible.

Therefore we may neglect $\gamma_{rad}(r_2)$ in equation (23) for all the levels with $r_2 > 4$ Å, which means $v \gtrsim 30$. For these levels r_1 is in the range 2.6-2.7 Å and we may easily evaluate $\gamma_{rad}(r_1)$:

$$-\,D_{BX}(r_1 = 2.65\text{ Å}) = 0.9\ (\text{Debye})^2\ (\text{Ref. [31]})$$

and

$$U_B(r = 2.65\text{ Å}) - U_X(r = 2.65\text{ Å}) = 19\,000\ \text{cm}^{-1}\,.$$

Thus we obtain $\gamma_{rad}(r_1) = 1.94 \times 10^6\ \text{s}^{-1}$ and the resulting theoretical value for $\Gamma_{rad}(v)$ is :

$$\Gamma_{rad}(v) = 0.97 \times 10^6\,\frac{\omega_v}{\omega_e}\,\text{s}^{-1}\,.$$

We have also tried to interpolate our results, using the same variation with v but with a fitted numerical factor ; our « best fit » is

$$\Gamma_{rad}(v) = 0.95 \times 10^6\,\frac{\omega_v}{\omega_e}\,\text{s}^{-1}\,. \qquad (26)$$

Both equations are in very good agreement ; we used equation (26) to plot the curve in figure 18, and for interpolation of Γ_{rad} in table VII. Although the present discussion is of great simplicity, we feel that it contains all the physical ideas and that the present agreement is by no means fortuitous.

5. **Conclusion.** — We have now a complete and coherent picture of the I_2 B state predissociation. It is the first case in which such an intricate predissociation has been studied in detail. We want to emphasize the following points :

— the great efficiency of dye lasers for such a study and the absolute necessity of extremely selective excitation ;

— the great variety of experiments necessary to characterize this predissociation.

Similar studies will probably appear soon ; for instance in Br_2 the corresponding B state predissociation has been observed [33]. These further studies will show more clearly what is general in our work on I_2 and what is more specific to this molecule.

Acknowledgments. — We are grateful to Mrs Lefebvre-Brion, to Professors C. Cohen-Tannoudji, J. P. Descoubes and to G. Grynberg for the help they have given us in the theoretical part of this work.

We thank F. Biraben and G. Gouedard for their help and advice in the experimental work.

Finally, we are indebted to Professor F. W. Dalby for many helpful discussions and his enthusiasm.

References

[1] STEUBING, W., *Verh. Dtsch. Phys. Ges.* (1913) 1181.
[2] WOOD, R. W. and RIBAUD, G., *Philos. Mag.* **27** (1914) 1009.
[3] TURNER, L. A., *Z. Phys.* **65** (1930) 464.
[4] VAN VLECK, J. H., *Phys. Rev.* **40** (1932) 544.
[5] DEGENKOLB, E. O., STEINFELD, J. I., WASSERMAN, E. and KLEMPERER, W., *J. Chem. Phys.* **51** (1969) 615.
[6] CHAPMAN, G. D. and BUNKER, P. R., *J. Chem. Phys.* **57** (1972) 2951.
[7] CAPELLE, G. A. and BROIDA, H. P., *J. Chem. Phys.* **57** (1972) 5027.
[8] BROYER, M., VIGUÉ, J. and LEHMANN, J. C., *Chem. Phys. Lett.* **22** (1973) 313.
[9] VIGUÉ, J., BROYER, M. and LEHMANN, J. C., *J. Phys. B* **7** (1974) L 158.
[10] VIGUÉ, J., BROYER, M. and LEHMANN, J. C., *J. Chem. Phys.* **62** (1975) 4941.
[11] BROYER, M., VIGUÉ, J. and LEHMANN, J. C., *J. Chem. Phys.* **64** (1976) 4793.
[12] VIGUÉ, J., Thesis, Paris (1978), unpublished.
[13] VIGUÉ, J., BROYER, M. and LEHMANN, J. C., *J. Physique* (article I of this series).
[14] VIGUÉ, J., BROYER, M. and LEHMANN, J. C., *J. Physique* (article II of this series).
[15] BARRAT, J. P. and COHEN-TANNOUDJI, C., *J. Physique Radium* **22** (1961) 329 and 443.
[16] GOUEDARD, G. and LEHMANN, J. C., *J. Physique* **34** (1973) 693.
[17] BROYER, M., LEHMANN, J. C. and VIGUÉ, J., *J. Physique* **36** (1975) 235.
[18] VIGUÉ, J., Thesis (3e cycle), Paris (1974), unpublished.
[19] HUO, W. M., *J. Chem. Phys.* **52** (1970) 3110.
[20] GERSTENKORN, S. and LUC, P., *Atlas du Spectre d'absorption de la molécule d'iode* (Edition du C.N.R.S.) 1978.
[21] BROYER, M., Thesis, Paris (1977), unpublished.
[22] TELLINGHUISEN, J., *J. Quant. Spectrosc. Radiat. Transfer* **19** (1978) 149.
[23] WEI, J. and TELLINGHUISEN, J., *J. Mol. Spectrosc.* **50** (1974) 317.
[24] CAPELLE, G. A. and BROIDA, H. P., *J. Chem. Phys.* **58** (1973) 4212.
[25] BROYER, M., VIGUÉ, J. and LEHMANN, J. C., *J. Chem. Phys.* **63** (1975) 5428.
[26] LEVENSON, M. D. and SCHAWLOW, A. L., *Phys. Rev.* **A6** (1972) 10.
[27] PAISNER, J. A. and WALLENSTEIN, R., *J. Chem. Phys.* **61** (1974) 4317.
[28] SHOTTON, K. C. and CHAPMAN, G. D., *J. Chem. Phys.* **56** (1972) 1012.
[29] GORDEEV, E. P., UMANSKY, S. Ya. and VORONIN, A. I., *Chem. Phys. Lett.* **23** (1973) 524.
[30] VIGUÉ, J., BROYER, M. and LEHMANN, J. C., *Phys. Rev. Lett.* **42** (1979) 883.
[31] TELLINGHUISEN, J., *J. Chem. Phys.* **48** (1973) 2821.
[32] BROOKE KOFFEND, J., BACIS, R. and FIELD, R. W., *J. Chem. Phys.* **70** (1979) 2366.
[33] ZARAGA, F., NOGAR, N. S. and BRADLEY MOORE, C., *J. Mol. Spectrosc.* **63** (1976) 564.
CLYNE, M. A. A. and HEAVEN, M. C., *Faraday Transactions* 2 **74** (1978) 1992.
LUYPAERT, R., DE VLIEGER, G. and VAN CRAEN, J., *J. Chem. Phys.* **72** (1980) 6283.
[34] DAS, G. and WAHL, A. C., *J. Chem. Phys.* **69** (1978) 53.
[35] BACIS, R., Private communication (1981).